Sideslip Angle Based Variable Slip Ratio Limiter for Direct Yaw Moment Control of Two-Input-Two-Output Motor Vehicles

Tona Sato[1], Takumi Ueno[1], Binh Minh Nguyen[1], Hiroshi Fujimoto[1], Hiromitsu Toyota[1,2], and Kaoru Sawase[2]

***Abstract*— This paper presents a new direct yaw moment control system for electric vehicles with two-input-two-output motor drives. The proposed system consists of two layers: yaw-rate control in the outer and driving force control in the inner. To optimize the driving force generation capability of the left and right tires during turning, a novel variable slip ratio limiter (VSRL) is developed for the driving force control (DFC). The VSRL algorithm is derived by analyzing the brush model of tire force characteristics concerning the sideslip angle of the vehicle body. The proposed system was evaluated using an actual electric vehicle prototype developed by Mitsubishi Motors. The experiments were conducted under extremely harsh conditions, such as sudden acceleration while cornering on the ice surface. Compared with the existing methods with conventional VSRL, the proposed system successfully enhances the yaw-rate tracking performance.**

I. Introduction

The growing environmental awareness helps shift from internal combustion engine vehicles (ICEVs) to electric vehicles (EVs). The motor, the driving force source of EVs, has advantages over ICEVs in environmental performance and vehicle motion control, such as significantly enhanced torque responsiveness and the ability to calculate the output torque from the motor current accurately [1].

EVs that can control the left and right wheels independently have the advantage of direct yaw moment control (DYC), which improves lateral stability [2]. Thanks to their high control bandwidth, in-wheel-motor EVs (IWM-EVs) have become the objectives of various advanced motion control approaches, such as anti-slip control [3], range extension control [4], and DYC [5], [6]. This paper focuses on DYC for on-board motor EVs (OBM-EVs). Although OBM-EVs are characterized by lower control bandwidth, there are examples of DYC being applied [7], [8].

Differential devices for OBM-EVs that can independently control left and right wheels have also been developed; one is a torque-difference-amplification torque vectoring differential (TDA-TVD) that combines two motors and many planetary gears. It has the advantage of amplifying the difference in driving forces between left and right. On the other hand, there are challenges regarding control performance due to the mechanical coupling [9], [10]. When the vehicle turns on slippery road surfaces, it needs additional considerations, such as driving force control (DFC) [11], [12]. In DFC, the primary correlation between the slip ratio and driving force is used for control. In general DFC, the slip ratio limiter is introduced to prevent wheel slippage [13]–[16]. The limiter is also set considering the optimal slip ratio of the straight driving, which produces the maximum driving force. Conventional DYC is quite effective in the gentle curve course. However, when the vehicle steers excessively, it reaches the grip limit, and the driving force difference is regulated, resulting in the loss of turning ability. Variable slip ratio limiter (VSRL) was proposed to deal with the above problem [17]. In [17], the slip ratio limiter of one side's wheel is fixed, and that of the other is varied based on the yaw moment reference. Unfortunately, [17] does not address the sideslip angle in the VSRL algorithm. The side on which the slip ratio limiter is fixed is considered the optimal slip ratio of just straight driving. However, the optimal slip ratio varies due to the slip angle while cornering [18]. Thus, the driving force generation capability might be degraded, especially when the vehicle turns on low friction roads, negatively influencing the yaw moment generation.

For the above discussion, this paper proposes a new DYC system for rear-wheel-drive EVs equipped with a TDA-TVD mechanism from the above discussion. The contribution of this paper is twofold. First, a hierarchical DYC control system is designed based on DFC. Second, it designed a new VSRL by thoroughly analyzing the tire force's brush model concerning the sideslip angle.

The remainder of this paper is organized as follows. In Section II, the vehicle motion model is formulated. In Section III, the design of the proposed VSRL algorithm is described. In Section IV, the proposed system is demonstrated by experiments using the real vehicle. Finally, the conclusion is stated in Section V.

II. Vehicle Dynamics Model

As shown in Fig. 1, the vehicle yaw motion is expressed as follows:

$$MV\left(\frac{d\beta}{dt}+\gamma\right) = 2(F_{yf}+F_{yr}+F_{yd}) \tag{1}$$

$$I\dot{\gamma} = N_z - N_t - N_d \tag{2}$$

where M and I denote body mass and yaw moment of inertia. V, γ, and β indicate the vehicle speed, yaw rate, and sideslip angle, respectively. Let F_y represent the lateral force acting

[1]Graduate School of Frontier Science, The University of Tokyo, 5-1-5 Kashiwanoha, Kashiwa, Chiba, 277-8561, Japan, fujimoto@k.u-tokyo.ac.jp

[2] MITSUBISHI MOTORS CORPORATION, 1, Nakashinkiri, Hashime-cho, Okazaki, Aichi 444-8501, Japan

*This work was supported by Mitsubishi Motors Corporation

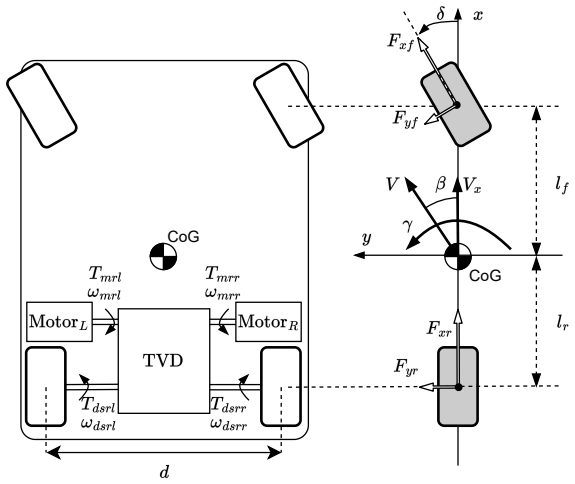

Fig. 1: TVD system placement and vehicle planar model

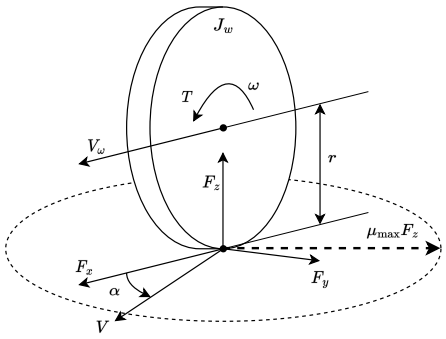

Fig. 2: One wheel model

on the tires, and F_{yd} the disturbance of the lateral force. The subscripts f and r denote the front and rear wheels. N_z is the moment generated by the difference in driving force. N_t and N_{dt} are produced by the lateral force and the yaw moment disturbance, respectively, and are given as follows:

$$N_t = 2(l_r F_{yr} - l_f F_{yf}) \tag{3}$$

$$N_{dt} = N_t + N_d \tag{4}$$

where l_f and l_r are the distances from the center of gravity (CoG) to the axles of the front and rear wheels, respectively.

The rotational motion of wheels, as shown in Fig. 2 is given as:

$$J_{\omega ij}\dot{\omega}_{ij} = T_{dsij} - rF_{xij} \tag{5}$$

where J_ω is the moment of wheel inertia, r is the wheel radius, ω is the wheel rotation speed, and T_{ds} is the torque acting on the drive shaft. As shown in Fig. 1, the torque output by the two motors is transmitted to the left and right drive shafts by the TVD system [9]. F_x also represents the longitudinal force acting on the tires, and the subscripts i and j denote the front/rear and right/left tire arrangement, respectively. The torque T_{ds} acts only on the longitudinal slip, the difference between the longitudinal body speed V_x and the wheel speed $V_w = r\omega$. The driving force F_x and lateral force F_y can be expressed as follows:

$$\begin{bmatrix} F_{xij} \\ F_{yij} \end{bmatrix} = F_{zij} \begin{bmatrix} C_{xij}\lambda_{ij} \\ C_{yij}\alpha_{ij} \end{bmatrix} \tag{6}$$

where C_x is driving stiffness, C_y is cornering stiffness, and F_z is vertical drag. The slip ratio λ is expressed as follows.

$$\lambda_{ij} = \frac{V_{\omega ij} - V_{xij}}{\max(V_{\omega ij}, V_{xij})} \tag{7}$$

In addition, α denotes the tire slip angle. The relationship holds for the sideslip angle β and α as follows:

$$\begin{bmatrix} \alpha_f \\ \alpha_r \end{bmatrix} = \begin{bmatrix} \beta - \delta \\ \beta \end{bmatrix} + \begin{bmatrix} l_f \\ -l_r \end{bmatrix} \frac{\gamma}{V} \tag{8}$$

III. Proposed Control Systems

A. Overview of control systems

Fig. 3 shows a block diagram of the proposed control system. The controller is composed of DYC and DFC. For the outer layer DYC, the yaw rate reference γ^* is expressed as follows:

$$\gamma^* = \frac{1}{1 + AV^2} \frac{V}{l_f + l_r} \delta \tag{9}$$

where δ is the steering rudder angle and A is the stability factor expressed as follows

$$A = -\frac{M}{2(l_f + l_r)^2} \frac{l_f C_{yf} - l_r C_{yr}}{C_{yf} C_{yr}} \tag{10}$$

The yaw moment reference value $\hat{N}_{in}$ is generated by the controller from the yaw rate reference. N_{dt} must be considered to improve robustness. The driving force difference moment reference is obtained by $N_z^* = N_{in}^* + \hat{N}_{dt}$ based on (2) and (4). The yaw moment constraint and disturbance N_{dt} are obtained by the following yaw-moment observer (YMO) equation using the driving force difference moment estimates [19]. where I_n is the nominal inertia and ω_c is the cutoff frequency. According to [9], the estimated driving force $\hat{F}_{xij}$ of the left and right rear wheels can be obtained by driving force observer (DFO). The driving force reference value F_{xij}^* for each wheel is obtained based on the following driving force distribution method using N_z^*, the driving force sum reference F_{xall}^* indicated by the accelerator pedal opening and tread d based on the force disturbance law (FDL) shown below.

$$\begin{bmatrix} F_{xrr}^* \\ F_{xrl}^* \end{bmatrix} = \begin{bmatrix} 1/2 & 1/d \\ 1/2 & -1/d \end{bmatrix} \begin{bmatrix} F_{xall}^* \\ N_z^* \end{bmatrix} \tag{11}$$

DFC has a cascade structure, including the wheel speed controller C_ω in the inner layer and the driving force controller C_f in the outer layer. DFC gives each wheel an appropriate torque. The slip ratio manipulation quantity y is defined as follows:

$$y = \frac{V_{\omega ij} - V_{xij}}{V_{xij}} \tag{12}$$

where y is the same definition as the slip ratio in deceleration.

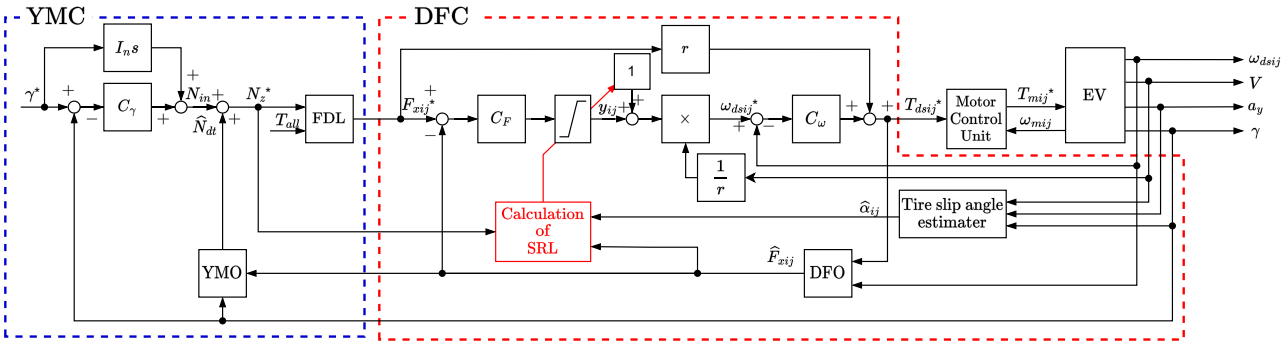

Fig. 3: Block diagram of the proposed DYC and DFC with proposal VSRL

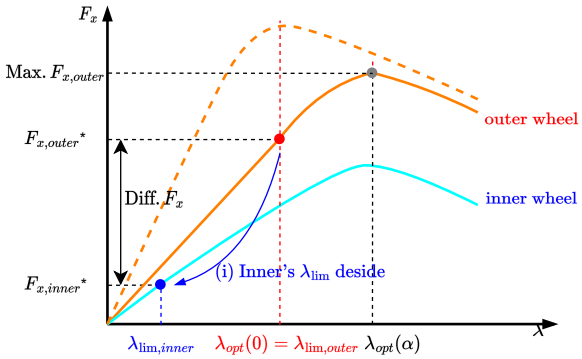

Fig. 4: Conventional variable slip ratio limiter

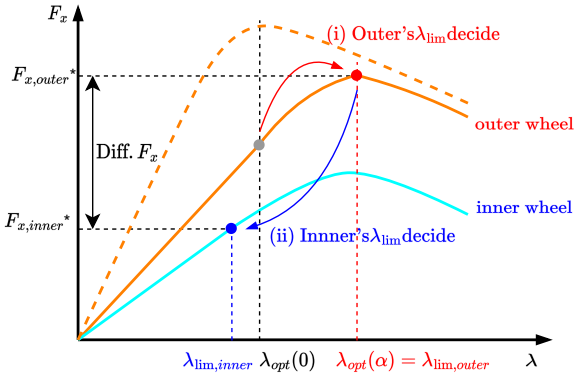

Fig. 5: Proposal variable slip ratio limiter

B. Conventional variable slip ratio limiter

Conventional yaw rate control that combines direct yaw moment control and driving force control saturates the driving force when the physical limit of the tire is used, and arbitrary driving force differential moments cannot be output, resulting in problems in tracking the yaw rate. Therefore, a variable slip ratio limiter for DYC was developed. This method fixes the optimal slip ratio $\lambda_{opt}(0)$ at the upper slip ratio α =0 rad on the outer side's wheel and reduces the upper slip ratio limit on the inner side's wheel according to the driving force moment reference based on (7) and (12).

$$[\lambda_{limr}, \lambda_{liml}] = \begin{cases} \left[\lambda_{opt}(0), \left(1 - \frac{2N_z^*}{d\hat{F}_{xrr}}\right)\lambda_{lim}(0)\right], & \text{(left turn)} \\ \left[\left(1 + \frac{2N_z^*}{dF_{xrl}}\right)\lambda_{opt}(0), \lambda_{opt}(0)\right], & \text{(right turn)} \end{cases} \tag{13}$$

Fig. 4 represents the workings of conventional VSRL.

C. Variable slip ratio limiter based on sideslip angle

The conventional VSRL did not take the sideslip angle into account. When the sideslip angle increases, the optimal slip ratio becomes more significant than $\lambda_{opt}(0)$, meaning that the conventional method cannot maximize the driving force. Therefore, as a new VSRL, the upper limit of the slip ratio on the outer wheel side is changed by the optimal slip ratio based on the inverse brush model using the sideslip angle. The driving force is expressed utilizing the brush model as follows:

$$F_x = \frac{\lambda}{\sqrt{\lambda^2 + \phi^2 \tan^2 \alpha}} F_{tire} \tag{14}$$

$$F_{tire} = \begin{cases} \mu F_z \eta(3 - 3\eta + \eta^2), & [0 \le \eta \le 1] \\ \mu F_z, & [\eta \ge 1] \end{cases} \tag{15}$$

where F_{tire} represent sum of force generated by a tire, ϕ is stiffness ratio of the tire expressed as C_x/C_y, μ is the coefficient of friction. According to [20], we can design a sideslip angle *beta* observer. Then, the tire slip angle α is obtained by (8). Assuming that traction control works effectively, the normalized tire-slip area η will never exceed $\eta > 1$, indicating that the entire tire contact surface area is completely idling. Then, the sum of forces generated by the tires, F_{tire}, is equal to the maximum driving force, $F_{x,\max}(0)$, when $\alpha = 0$. Using this, the normalized slip ratio $\lambda' = \lambda(\alpha)/\lambda_{opt}(0)$ expresses as follows.

$$f(\lambda') = \frac{F_x(\alpha)}{F_x(0)} = \frac{\lambda'}{\sqrt{\lambda'^2 + 1/\lambda_{opt}(0) \tan^2 \alpha}} \tag{16}$$

If $\frac{\partial f(\lambda')}{\partial \lambda'} = 0$, λ' has the maximum driving force. However, the approximate solution is infinite. Therefore, $\frac{\partial f(\lambda')}{\partial \lambda'} \le \epsilon$, the driving force is considered to be maximum at the threshold.

$$\frac{\partial f(\lambda')}{\partial \lambda'} = \frac{\left(1/\lambda_{opt}^2(0)\right) \tan^2 \alpha}{\left(\left(1/\lambda_{opt}^2(0)\right) \tan^2 \alpha + \lambda'^2\right)^{3/2}} \le \epsilon \tag{17}$$

TABLE I: Vehicle Parameter

Symbol	Description	Value
M	Vehicle Mass	2100 kg
J	Inertia of Wheel	2.0 kgm^2
r	Wheel of radius	0.363 m
$\lambda_{opt}(0)$	Optimal slip ratio at slip-angle=0 rad	0.06

Fig. 6: Experimental vehicle

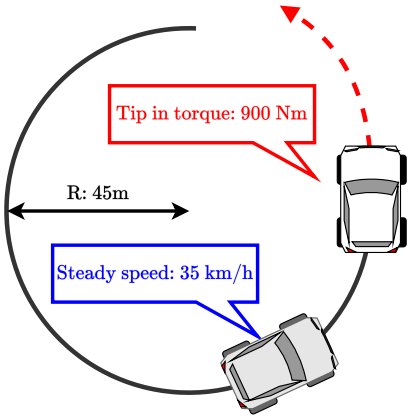

Fig. 7: Experimental scenario

From (17), $\lambda_{opt}(\alpha)$ is obtained as follows

$$\lambda_{opt}(\alpha) = \sqrt{\left|\left(\frac{\tan^2\alpha}{\lambda_{opt}^2(0)\epsilon}\right)^{2/3} - \left(\frac{\tan^2\alpha}{\lambda_{opt}^2(0)}\right)\right|}\lambda_{opt}(0) \tag{18}$$

From (13) and (18), the upper slip ratio limits for the left and right sides are defined as follows.

$$[\lambda_{limr}, \lambda_{liml}] = \begin{cases}\left[\lambda_{opt}(\alpha), \left(1 - \frac{2N_z^*}{d\hat{F}_{xrr}}\right)\lambda_{opt}(\alpha)\right], & \text{(left turn)} \\ \left[\left(1 + \frac{2N_z^*}{dF_{xrl}}\right)\lambda_{opt}(\alpha), \lambda_{opt}(\alpha)\right], & \text{(right turn)}\end{cases} \tag{19}$$

(i) and (ii) in Fig. 5 visually represents the process of determining the upper slip ratio limits for the outer and inner rings, respectively.

IV. Experiment

A. Experimental vehicle

To confirm the effectiveness of the proposed method, an experiment was conducted by Mitsubishi Motor Corporation using an EV equipped with a TDA-TVD system, as shown in Fig. 6. The parameters that can be disclosed are listed in Table 1. Although this vehicle was originally 4WD, in this paper, the front wheels are considered driven wheels because of the direct yaw moment control of only the rear wheels, and the average value was used as the vehicle body speed.

B. Experimental conditions

The experimental vehicle was tested by running as shown Fig. 7 and the following: A steady circle turn was performed at 35 km/h and radius 45 m on a slippery pressurized snow-turning road, and tip-in acceleration with 900 Nm of torque sum was performed without scanning the steering angle to compare the turning behavior. By the fitting process, the proportional and integral gains of the wheel speed controller C_ω were set to be 8.01 and 0.12, and the integral gain of the driving force controller C_f was set to be 0.001. For the yaw moment controller, the proportional gain of the yaw rate controller C_γ was set to 0.001, and the cutoff frequency of the yaw moment observer was set to 30 Hz. Also, the sideslip angle observer was calibrated, and poles were determined based on the data obtained from the V-BOX. The constraint condition ϵ for the optimal slip ratio gradient of the proposed method was set to 0.3. Four cases, including the proposed method, were run three times each. Data was collected as follows: Case 1: Simply torque input (Torque sum command given equally to left and right), Case 2: DFC and DYC (upper slip ratio limit fixed at 0.1 for both right and left), Case 3: DFC, DYC, and the VSRL proposed by [17] (fixed upper slip ratio limit on outer ring side, variable on inner ring side), and Case 4: VSRL based on DFC, DYC and sideslip angle (Proposed method). The $\lambda_{opt}(0)$ was also set to 0.06, the steady circle turn value that could be performed without breaking down in Case 2.

C. Experimental results

Fig. 8- 11 show each case's slip ratio, yaw rate, driving force sum, and yaw moment result. The timing of chip-in acceleration is at 1 second in the graph. In Case 1, the wheels are largely slipping, and the yaw rate diverges due to loss of lateral grip. In Cases 2 and 3, the slip ratio saturates at the 4-second point, and the target driving force difference cannot be output, leaving the understeer characteristic. In contrast, the proposed Case 4 method can output any driving force differential and recover from understeer at 4 s.

Also, focusing on (c), it can be seen that the proposed method has the highest peak driving force on the outer wheel. In addition, to evaluate the effort of the proposal method numerically, Fig.12 and 13 show the root mean square error (RMSE) of the yaw rate and yaw moment. The reason why Case 1 is not shown in Fig. 13 is that, as shown in Fig. 8, the yaw moment reference is not used in Case 1, such as Fig.6 shows that the yaw moment command is not used in case 1. The smaller the value, the more influential the tracking control is. Fig. 12 shows that is. 9.1% and 34% reductions in RMSE were observed in Case 2 and Case 3, respectively, based on Case 1, while a 62% reduction was achieved in Case 4 using the proposed method.

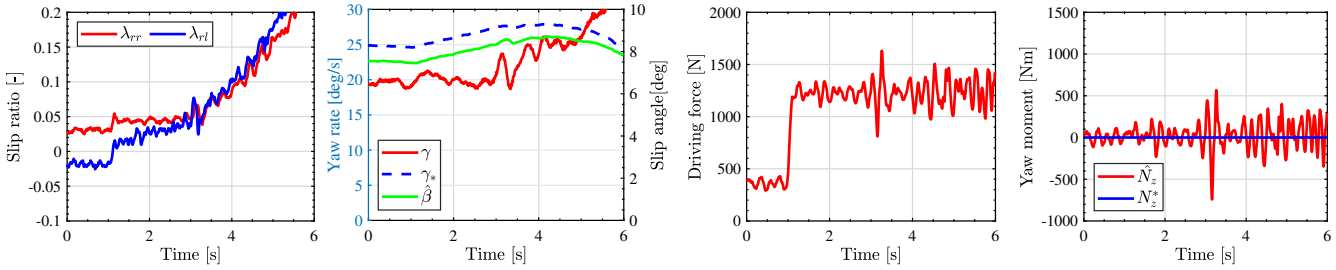

(a) Slip ratio (b) Yaw rate and sideslip angle (c) Driving force of outer wheel (d) Yaw moment

Fig. 8: Experimental result of Case 1 (Simply input)

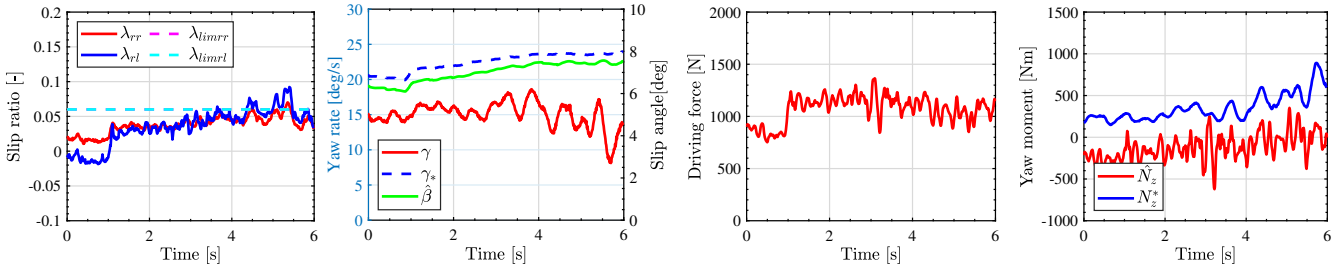

(a) Slip ratio (b) Yaw rate and sideslip angle (c) Driving force of outer wheel (d) Yaw moment

Fig. 9: Experimental result of Case 2 (DYC & DFC)

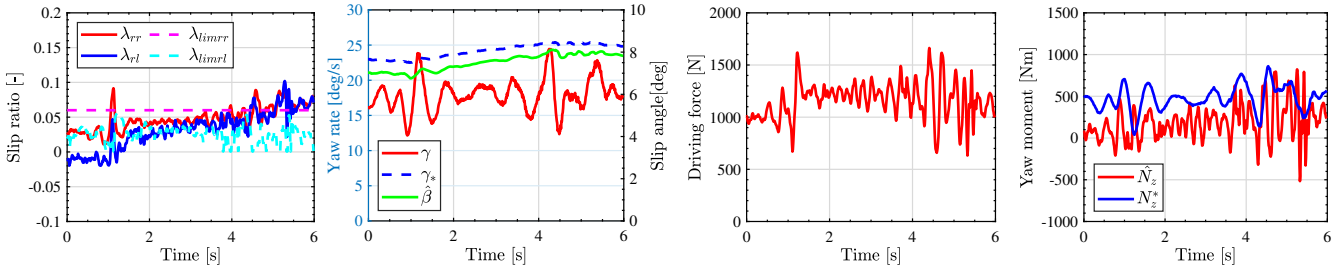

(a) Slip ratio (b) Yaw rate and sideslip angle (c) Driving force of outer wheel (d) Yaw moment

Fig. 10: Experimental result of Case 3 (DYC & DFC with conventional VSRL)

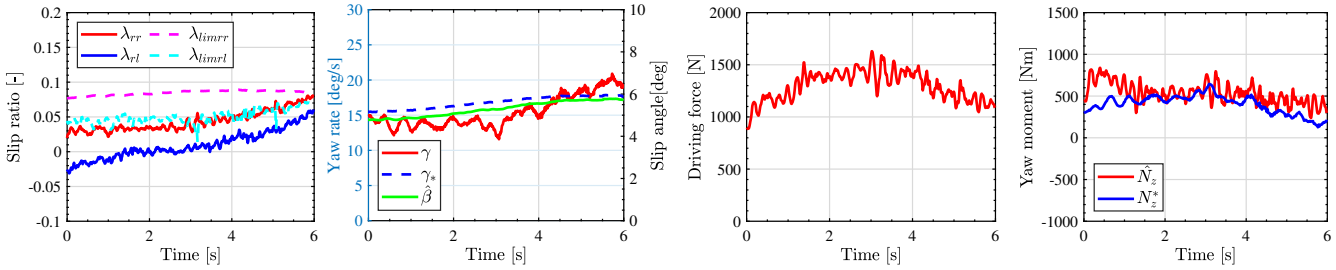

(a) Slip ratio (b) Yaw rate and sideslip angle (c) Driving force of outer wheel (d) Yaw moment

Fig. 11: Experimental result of Case 4 (DYC & DFC with proposal VSRL)

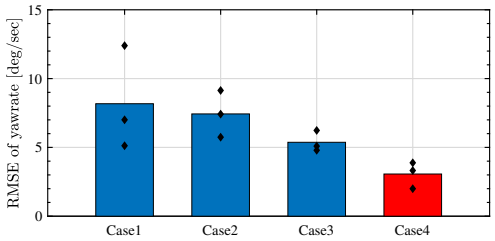

Fig. 12: RMSE of yawrate

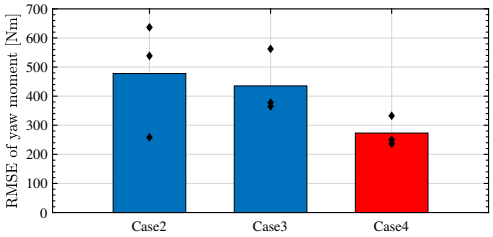

Fig. 13: RMSE of yaw moment

V. Conclusion

In this study, we proposed the new VSRL considering the sideslip angle. The experimental results show that the proposed method can ensure excellent vehicle yaw stability by varying the upper slip ratio limiter based on the sideslip angle, even in a limit state when the physical limit saturates the driving force. The proposed method also has superior acceleration performance compared to the conventional method, combining vehicle stability and acceleration performance. However, this method cannot cope with changes in the optimal slip ratio due to road conditions. Combined with estimating the optimal slip ratio, this controller can be used in more diverse situations.

Acknowledgement

We appreciate that Mitsubishi Motors Corporation supported this study and thank them for graciously allowing us to use their test site and vehicle.

References

[1] L. Hua, J. Tang, H. Dourra, and G. Zhu, "A gray-box surrogate vehicle energy consumption model capable of real-time updating," *IEEE/ASME Transactions on Mechatronics*, vol. 28, no. 4, pp. 2092–2100, 2023.

[2] T. Shen, G. Yin, Y. Ren, F. Wang, B. Feng, and J. Liang, "Stability and maneuverability guaranteed torque distribution strategy of ddev in handling limit: A novel lstm-lmi approach," *IEEE/ASME Transactions on Mechatronics*, vol. 27, no. 6, pp. 5647–5658, 2022.

[3] Z. Zhang, C. guang Liu, X. jun Ma, Y. yin Zhang, and L. ming Chen, "Driving force coordinated control of an 8×8 in-wheel motor drive vehicle with tire-road friction coefficient identification," *Defence Technology*, vol. 18, no. 1, pp. 119–132, 2022.

[4] Y. Ikezawa, H. Fujimoto, Y. Hori, D. Kawano, Y. Goto, M. Tsuchimoto, and K. Sato, "Range extension autonomous driving for electric vehicles based on optimal velocity trajectory generation and front-rear driving-braking force distribution," *IEEJ Journal of Industry Applications*, vol. 5, no. 3, pp. 228–235, 2016.

[5] D. Liu, S. Huang, S. Wu, and X. Fu, "Direct yaw-moment control of electric vehicle with in-wheel motor drive system," *International Journal of Automotive Technology*, vol. 21, pp. 1013–1028, 2020.

[6] L. Jiang, S. Wang, J. Meng, X. Zhang, J. Jin, and Y. Xie, "Inverse decoupling-based direct yaw moment control of a four-wheel independent steering mobile robot," in *2020 IEEE/ASME International Conference on Advanced Intelligent Mechatronics (AIM)*, 2020, pp. 892–897.

[7] L. De Novellis, A. Sorniotti, P. Gruber, J. Orus, J.-M. Rodriguez Fortun, J. Theunissen, and J. De Smet, "Direct yaw moment control actuated through electric drivetrains and friction brakes: Theoretical design and experimental assessment," *Mechatronics*, vol. 26, pp. 1–15, 2015.

[8] J. Persson and J. Åkesson, "On torque vectoring to improve steering predictability while minimising power loss in heavy electric vehicles using model predictive control," 2023.

[9] G. Yu, H. Fuse, H. Fujimoto, K. Sawase, N. Takahashi, R. Takahashi, Y. Okamura, and R. Koga, "Feedback control design for drive shaft vibration suppression based on frequency domain analysis of two-input-two-output motor drive system," in *IECON 2022–48th Annual Conference of the IEEE Industrial Electronics Society*. IEEE, 2022, pp. 1–6.

[10] H. Fuse, H. Fujimoto, K. Sawase, N. Takahashi, R. Takahashi, Y. Okamura, and R. Koga, "Derivation of dynamic model of two-input-two-output torque difference amplification motor drive system and independent left-and-right wheel control with decoupling compensator," *IEEJ Journal of Industry Applications*, vol. 11, no. 3, pp. 427–436, 2022.

[11] H. Fujimoto, T. Saito, and T. Noguchi, "Motion stabilization control of electric vehicle under snowy conditions based on yaw-moment observer," in *The 8th IEEE International Workshop on Advanced Motion Control, 2004. AMC '04.*, 2004, pp. 35–40.

[12] R. Rajamani, N. Piyabongkarn, J. Lew, K. Yi, and G. Phanomchoeng, "Tire-road friction-coefficient estimation," *IEEE Control Systems Magazine*, vol. 30, no. 4, pp. 54–69, 2010.

[13] X. Sun, Y. Wang, Y. Cai, P. K. Wong, L. Chen, and S. Bei, "Nonsingular terminal sliding mode-based direct yaw moment control for four-wheel independently actuated autonomous vehicles," *IEEE Transactions on Transportation Electrification*, vol. 9, no. 2, pp. 2568–2582, 2023.

[14] G. De Filippis, B. Lenzo, A. Sorniotti, P. Gruber, and W. De Nijs, "Energy-efficient torque-vectoring control of electric vehicles with multiple drivetrains," *IEEE Transactions on Vehicular Technology*, vol. 67, no. 6, pp. 4702–4715, 2018.

[15] B. Lenzo, M. Zanchetta, A. Sorniotti, P. Gruber, and W. De Nijs, "Yaw rate and sideslip angle control through single input single output direct yaw moment control," *IEEE Transactions on Control Systems Technology*, vol. 29, no. 1, pp. 124–139, 2020.

[16] Z. Li, H. Chen, H. Liu, P. Wang, and X. Gong, "Integrated longitudinal and lateral vehicle stability control for extreme conditions with safety dynamic requirements analysis," *IEEE Transactions on Intelligent Transportation Systems*, vol. 23, no. 10, pp. 19 285–19 298, 2022.

[17] T. Ueno, B.-M. Nguyen, and H. Fujimoto, "Direct yaw moment control for electric vehicles with variable-rate-slip-ratio-limiter based driving force control," in *2023 IEEE International Conference on Mechatronics (ICM)*, 2023, pp. 1–6.

[18] E. Hashemi, M. Jalali, A. Khajepour, A. Kasaiezadeh, and S.-k. Chen, "Vehicle stability control: Model predictive approach and combined-slip effect," *IEEE/ASME Transactions on Mechatronics*, vol. 25, no. 6, pp. 2789–2800, 2020.

[19] Y. Wang and H. Fujimoto, "Yaw moment observer design for electric vehicles considering vehicle speed variation," in *the 12th International Symposium on Advanced Vehicle Control*, 2014.

[20] B. M. Nguyen, Y. Wang, H. Fujimoto, and Y. Hori, "Sideslip angle estimation using GPS and disturbance accommodating multi-rate kalman filter for electric vehicle stability control," in *2012 IEEE Vehicle Power and Propulsion Conference*. IEEE, 2012, pp. 1323–1328.